Aerospace Europe Conference 2023 - $10^{th}$ EUCASS - $9^{th}$ CEAS

DOI: ADD DOINUMBER HERE

# Preliminary analysis of the magnetic arch plasma expansion in a cluster of two ECR plasma thrusters

*Célian Boyé*[⋆†], *Jaume Navarro-Cavallé*[⋆] *and Mario Merino-Martinez*[⋆]
[⋆]*Equipo de Propulsóin Espacial y Plasmas (EP2), Universidad Carlos III de Madrid*
*Leganés, Spain*
cboye@ing.uc3m.es · janavarr@ing.uc3m.es · mario.merino@uc3m.es
[†]Corresponding author

## Abstract

An electric propulsion device clustering two coaxial Electron Cyclotron Resonance Thrusters (ECRTs) driven by microwaves at 2.45 GHz with a closed-line magnetic field is studied. The characterisation of a single source composing the cluster has been realised beforehand. The plasma expansion in the closed-line magnetic field arch formed in a cluster of two ECRTs is placed at the centre of the study, to assess the viability of the clustering of Electrodeless Plasma Thrusters (EPTs). The characterisation of the cluster has been realised with three different magnetic topologies, Krypton and a mass flow rate of 15 sccm (100 W). The closed-line magnetic field topology does not prevent plasma extraction and acceleration, demonstrated by the comparison of the performances between the single ECR source and the cluster of two ECR sources.

## 1. Introduction

In recent years, Electrodeless Plasma Thrusters (EPTs) have been a subject of focus in the electric propulsion field, in contrast to classic and more predominant thrusters such as Hall effect thrusters (HETs) or Gridded Ion Engines (GIEs).[1–3] EPTs regroup various concepts, two of them being Helicon Plasma Thrusters (HPTs) or Electron Cyclotron Resonance Thrusters (ECRTs). Ionisation occurs in EPTs with the use of electromagnetic waves in the $MHz$ range for the HPTs[4–8] and the $GHz$ range for the ECRTs.[9–11] ECRTs couple microwaves with a magnetic field to heat the electrons by resonant absorption. Besides, plasma can be accelerated and carried out of these thrusters with a magnetic nozzle (MN). The MN also confine the plasma, hence reducing the particle losses on the walls. The absence of an electrode in contact with the plasma for ionisation or acceleration reduces erosion and performance degradation. Moreover, EPTs are neutraliser-free thrusters due to their current-free plume. This offers potential advantages in terms of simplicity, operational flexibility, lifetime, and the possibility of operating on multiple propellants. However, it is to be noted that EPTs present some disadvantages. Indeed, they present lower $I_{sp}$ and thrust efficiency compared with HETs or GIEs, combined with a higher plume divergence. Development and studies are still needed for EPT to leave the prototype stage and face classic propulsion systems in the new space propulsion field.[8,12] Once the plasma is generated by ECR, the MN coil produces a magnetic field to enable the plasma acceleration and expansion outside of the thruster, using part of the coupled microwave power transformed into kinetic energy[13–15] to generate thrust.

ECRT concepts have been developed since the 1960s, with different power transmission lines, propellants, microwave working frequencies and geometries. It had been proven by Miller that a coupling up to 90% of the microwave power into the plasma can be reached (2.45 GHz, 320 W with Argon).[16–19] The impact of the magnetic field topology and the ionisation region position was demonstrated by Kosmahl.[20] Sercel produced several works denoting the limits of ECRT in the California Institute of Technology.[21–24] Achieving high mass efficiency (85%) with low power and divergence efficiencies (< 30%), Sercel highlighted the important effect of the background pressure, the wall losses; and the need to improve the magnetic nozzle to decrease the divergence of the plasma beam. The latest major investigations on ECRT have been conducted by ONERA,[25–28] based on a coaxial ECRT in the framework of the MINOTOR project. This new geometry differs from the usual waveguide ECRT, enabling the use of a lower power-to-mass flow rate ratio. Thrust efficiencies in the 30% – 50% range have been reached,[28,29] as well as the strong link in between the $Xe^+$ ion energy and the pressure inside the ionisation chamber (IC).[25,26] Moreover, thruster efficiency has been increased significantly.[27] However, the presence of a coaxial central conductor implies erosion and metallic deposition on the rear plate, limiting the lifetime of the prototypes regarding classic waveguide ECRT.[30,31] These latter have been furthermore investigated in various works, especially regarding their higher power range capability and the possibility

to overcome the limited lifetime of coaxial ECRT.[32,33] It is to be taken into account that coaxial ECRTs are not electrodeless, due to the presence of a stainless steel coaxial cylinder immersed in the plasma. Moreover, the simplicity of coaxial ECRT design led to the use of the latter in the present work to ease design iterations and development. As it will be detailed in Section 2, the sources used in this study comprise a main coil localised behind the IC (Back coil - BC) and a magnetic nozzle coil (MN) placed near the plasma exhaust plane. The coils are respectively responsible for providing the resonance field to enable the ECR and to accelerate and carry the plasma out of the IC. Existing EPT, and more especially ECRT, consist of a cylindrical discharge chamber with a MN localised at the plasma exhaust plane. The latter forms a magnetic field consisting of diverging magnetic lines. This magnetic field not only imprints a high divergence angle to the plasma beam but creates a high-energy plasma environment around the spacecraft.[34] Moreover, it interacts with the geomagnetic field, creating a magnetic torque on the spacecraft.

A cluster of two ECR sources with opposing polarities placed side by side forms a magnetic arch (MA) - designating a closed-line magnetic field geometry. The closed-line topology and near-zero net dipole would lower the magnetic torque when interacting with the geomagnetic field and the magnetic interference with the spacecraft. Nevertheless, clustering two EPTs with a MA rises the question of whether it is possible to extract plasma from the closed-line magnetic field. Recent studies have been tackling this issue. The behaviour and the effect of such a magnetic topology have not been experimentally studied yet. To begin with, an experimental clustering of an EPT has been realised by Vereen et al.[35],[36] under the supervision of Winglee at the University of Washington. Though, only the clustering of two HPT sources joined in one exhaust has been realised. The goal of mentioned studies was indeed defined as extending the power regime of a single HPT.[35] Thus, the diverging magnetic field has been the only one characterised in this work. A main simulation work on EPTs clustering has been realised by Merino et al. in 2022, on ECRT. 3D simulation works have been performed in 2023 Di Fede et al.[37] on HPT. MA has been a subject of study, as well as other magnetic topologies. Both works show promising and interesting results, encouraging deeper and more accurate simulation works to achieve a better understanding of EPT clustering. The clustering made by Vereen et al.[3536] consisted in the clustering of two HPTs in one exhaust with a single magnetic nozzle. Thus, no MA could be generated by the clustered HPH system. Thus, the experimental characterisation of the MA remains a novelty, as well as the first ignition of a cluster composed of two EPTs.

This work aims to validate experimentally the operation of a magnetic arch, formed when two ECRTs are fired together with different polarities. To this end, we propose an experimental setup consisting of two coaxial ECRTs, and an RPA mounted on a rotating arm as a first approach to characterising the plasma expansion at the magnetic arch. After characterising a single source, we present the ion current density and ion energy measurements of the two sources with identical and opposing polarities, as well as in the absence of a magnetic field. The goal of these measurements resides in showing that a plasma beam can indeed be extracted from the closed-line MA topology (opposing polarities), with high current density and smaller divergence than with identical polarities, albeit with a slightly lower ion energy.

The rest of the document is organised as follows. Section 2 depicts the ECR source and the cluster composed of two ECR sources, as well as the experimental setup circumambient these latter - such as the transmission line, intrusive plasma probes or the vacuum chamber facility. In Section 3, measurements obtained by the intrusive plasma probes are discussed. To finish with, Section 4 refers to the conclusions drawn from the ECR sources cluster characterisation.

## 2. Experimental setup

### 2.1 ECR source description

The ECR sources used in these experiments are shown in Figure 1. A single source can be decomposed into the following main parts: two electromagnets, gas injection, power injection and ionisation chamber. The main characteristics and operational parameters of both thrusters can be seen in Table 1.

The central element of a source remains the ionisation chamber (IC), indicated in Figure 1. As mentioned in Table 1, this stainless steel assembly is 43.73 mm long for an internal diameter of 30mm. To transmit microwave power, a 6 mm diameter stainless steel coaxial cylinder is placed at the centre of the IC. The inductor is threaded to an M3 core coaxial termination, connecting it to the transmission line thanks to a 7-16 DIN panel crimp. A pierced alumina disk sealed with ceramic paste is placed right after the panel crimp ending to protect the back of the source from plasma. The IC is held tight with a dielectric holding system to keep the latter floating. The floating potential of the IC was monitored at all times by a multimeter, thanks to a wire attached to one of the mounting screws of the IC.

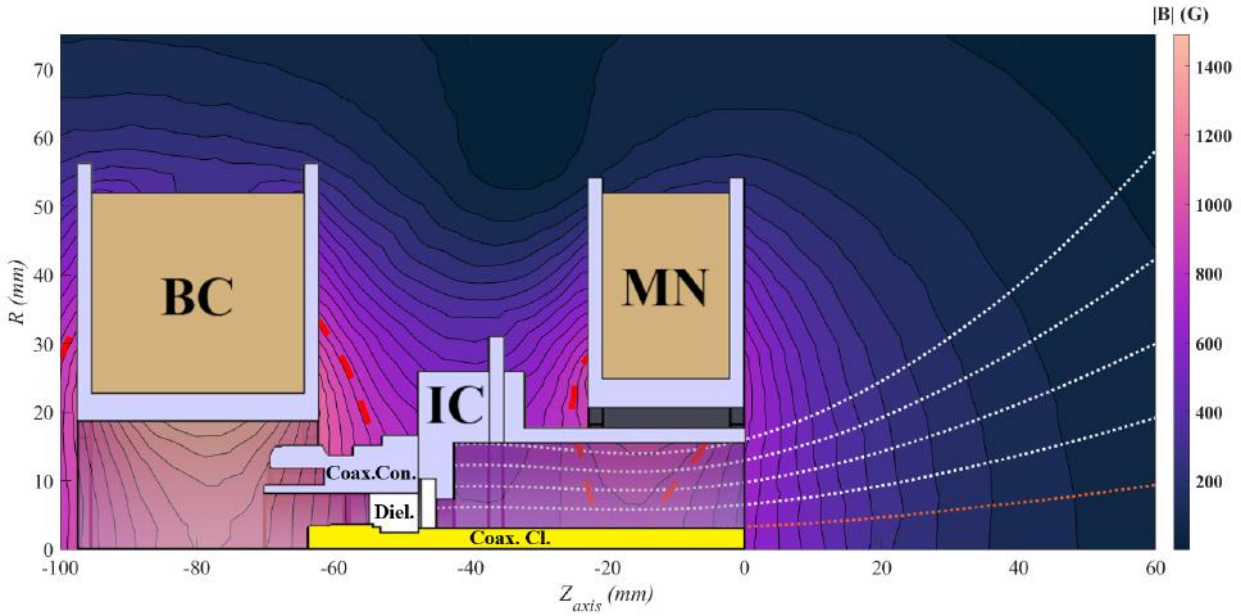


Figure 1: 2D magnetic field streamlines plot of one source. Red dashed lines represent the ECR resonance surfaces at 875 G. White dot lines represent the magnetic field streamlines coming from the rear plate of the ionisation chamber (IC). The orange dot line represents the magnetic field streamlines generated at the base of the coaxial cylinder. CAD of the ECR source is superposed. The IC, the back coil (BC), the magnetic nozzle coil (MN), the dielectric shield (Diel.), the panel crimp coaxial connector (Coax. Con.) and the coaxial cylinder (Coax. Cl.) are shown. The transmission line is localised behind the IC, beginning with the coaxial cable linking the panel crimp coaxial connector with the coaxial splitter for the cluster and with the DC block for the single source.

Figure 1 depicts the magnetic field topology generated by the ECR source. The BC and MN electromagnets are respectively responsible for the generation of the magnetic field to allow the ECR (875 G) and for the expansion of the magnetic topology out of the source. They are made of 1 mm enamelled copper wire, with a total number of turns of 1200 per source. The magnetic field topology can be modified thanks to the MN electromagnet. However, both have to be used to achieve the minimum magnetic field strength required to reach ECR resonance. The resonance condition is crossed at the very base of the coaxial cylinder, as well as halfway through the IC. The use of electromagnets brings flexibility during the operation of the thruster as the resonance surface can be displaced and the magnetic topology can be modified simply by varying current. Each electromagnet is controlled independently thanks to multiple independent power supplies. Measurements on a single source have been done with and without magnetic field, referenced respectively as *MF ON* and *MF OFF*. To obtain a symmetric plasma plume out of the cluster, the corresponding pair is powered with the same current. For the cluster configuration, two magnetic topologies have been defined: *MF ARCH* and *MF SAME*. The *MF ARCH* topology defines the configuration in which a closed-line magnetic field is produced by reversing the polarity of the electromagnets of one source, as shown in the left part of Figure 2. The *MF SAME* topology consists of the two sources with electromagnets polarised in the same direction, as it can be noticed in the right part of Figure 2. The *MF ARCH* remains the main configuration to be studied because of the closure of the magnetic field.

Krypton has been used as a propellant during the characterisation of the two thrusters. Each source implements a one-hole injection on the upper part of the IC, as shown in Figure 3. One-hole type injections are known to bring asymmetry and inhomogeneity in the plasma plume.[38] Still, they are used in the current source design to simplify manufacturing. The gas injection connection is not made independent for each source, as splitting is performed thanks to a Swagelok T-shape connector higher in the gas injection line. Thus, in this setup, a small mass flow imbalance might arise between the two sources.

| | |
|---|---|
| **Ionisation chamber length** | 43.73 mm |
| **Ionisation chamber internal diameter** | 30 mm |
| **Inductor length** | 46 mm |
| **Inductor length immersed in plasma** | 43.73 mm |
| **Inductor diameter** | 6 mm |
| **Maximum electromagnet power per source** | 1 kW |
| **Total number of turns per source** | $\approx$ 1200 |
| **ECR magnetic field** | 875 G |
| **Maximum magnetic field** | 1480 G |
| **Microwave power range** | 50 – 500 W |
| **Mass flow rate range (Kr)** | 7.5 – 50 sccm |

Table 1: Single ECR source and cluster of two ECR sources main characteristics and operational parameters.

The transmission line (TL) used to carry microwave power to the thruster is composed of several elements linked by coaxial cables. Even though coaxial cables imply limitations in terms of maximum power and heating issues, their use has been motivated by their flexibility in assembly and procurement. The 7-16 DIN standard has been taken as a reference in terms of coaxial connection, as it allows greater power to be transmitted at 2.45 GHz than most of the usual coaxial connection types. Microwave power is generated by a MR1000D-200ML 2.45 GHz ± 50 MHz solid-state Microwave Generator (MWG) from Muegge. The power is transmitted through the vacuum chamber thanks to a 2.45 GHz Allectra 242-7 16-K50 feedthrough before it reaches a total DC-block made of two RFWA340D9CFAL Coaxial to Waveguide (C2W) adapters. To fit with the 2.45 GHz microwave, rectangular flanges with the WR340 standard have been used. The C2W are separated by 1 mm, electrical insulation being maintained by ceramic washers. The goal of using such a DC block relies on the necessity to keep the IC electrically floating. Near-perfect transmission of the microwave has been measured through the DC block, with leaks under 0.1% of the power. The main difference between these TL is the 3dB D2-16FD coaxial three ways splitter from Microlab placed before the sources to divide equally the microwave power. Two TL have been used, respectively for the single source and cluster (Figure 4). The TL of the single ECR source is a simplified version of the one of the cluster, without the coaxial splitter.

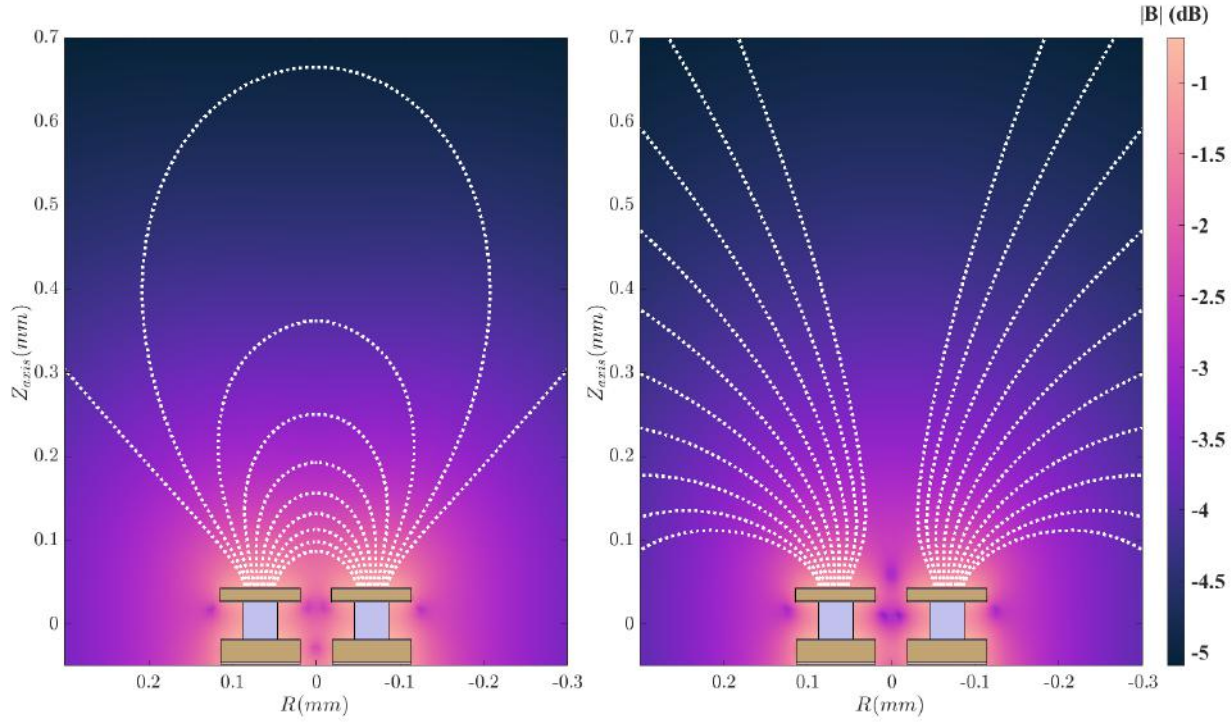


Figure 2: 2D magnetic field topology of the *MF ARCH* configuration (left) and *MF SAME* configuration (right). Magnetic field simulations were done on MatLab. Magnetic field lines are drawn in black, BC electromagnets in green, MN electromagnets in red and ionisation chamber (IC) in blue.

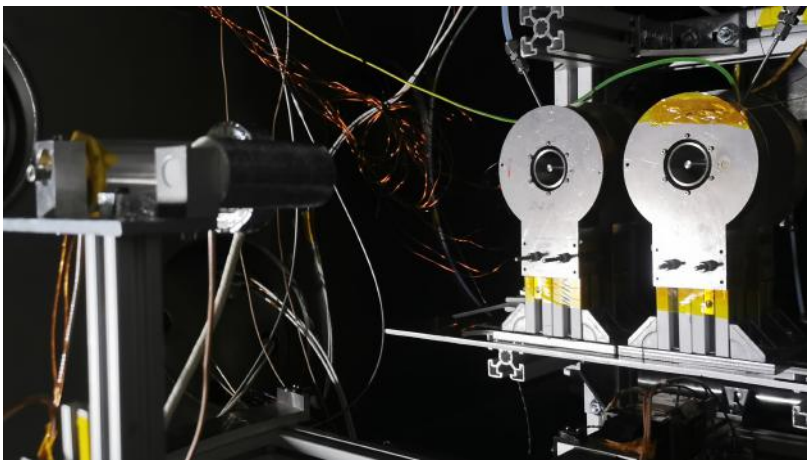

Figure 3: Picture of the assembled ECR cluster with electrostatic probes in front. The gas injection can be noticed on top of the sources' ionisation chamber.

The MR1000D-200ML solid-state generator includes a circulator and a dummy load, protecting it from reflected waves. Moreover, it allows us to measure the set ($P_{set}$), forwarded ($P_F$) and reflected ($P_R$) powers in the TL. $P_{set}$ can be directly set on the MWG, the latter also returning $P_F$ and $P_R$. Thanks to the transmission coefficient $\gamma$, it is possible to estimate the power delivered to the thruster thanks to the relation $P_T = |S_{12}|^2 P_F - |S_{12}|^{-2} P_R$. The transmission coefficient $|S_{12}|$ has been determined by analysing the TL from the output of the MWG to the input of the splitter with a Virtual Network Analyser (VNA), and has been determined to be: $|S_{12}| = 0.8443$. The transmission coefficient does not include the losses linked to the coaxial splitter and remains an approximation of the total amount of power received by the sources of the cluster.

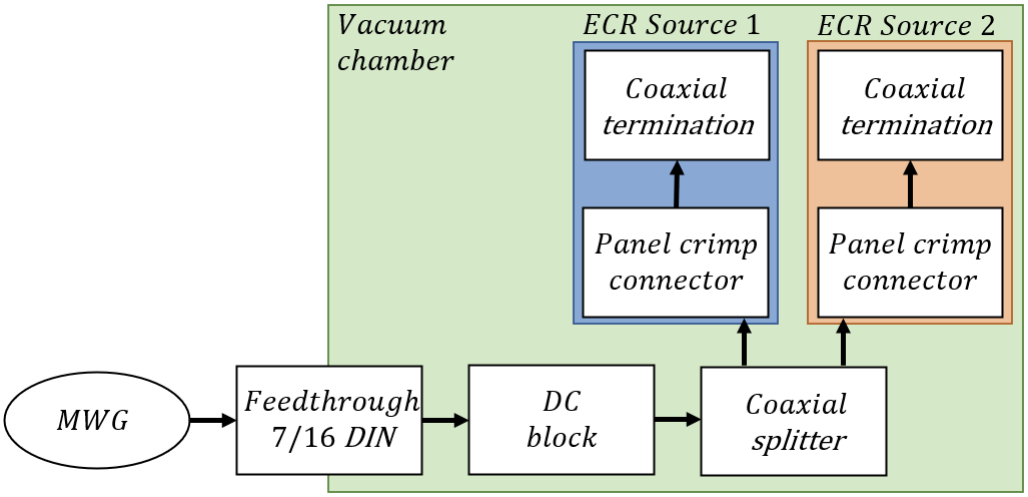


Figure 4: Transmission line scheme for the two ECR sources cluster.

Moreover, heating has been observed on the elements of the TL during operation. Heating worsens the TL transmission quality by increasing the insertion losses and modifying the transmission properties. Another issue faced with the use of microwaves remains the radiation from the thruster after the microwave generator is turned on but before the plasma discharge is initiated. Protections have been set up on the windows of the vacuum chamber, such as metallic grids with sufficiently fine meshing to block microwaves. In addition, a leak detector has been used at all times during the experiments to ensure the absence of microwaves leaking from the chamber.

### 2.2 Experimental facilities

The vacuum chamber used to test both the single source and the cluster is placed at the Laboratory of Space Propulsion of Universidad Carlos III de Madrid (or UC3M). It consists of a stainless-steel vessel of 3.5 m in length and a 1.5 m inner diameter. Three types of pumps are in use: one main dry pump Leyvac LV80 (capacity of 80 $m^3$/h), two turbomolecular pumps Leybold MAGW2.200iP (capacity of 2000 l/s) and three cryopanels Leyvac 140 T-V (capacity of 37000 l/s for Xenon). In dry conditions, pressures in the order of magnitude of $10^{-7}$ mbar can be reached. With 50 sccm of Krypton in the vacuum chamber injected for ignition of the cluster, pressure rises to $10^{-5}$ mbar - to stabilise around $10^{-5}$ mbar when 15 sccm is injected during nominal operation. The exhausts of the sources have been placed at 2 m away from one end of the vacuum chamber, to minimise the effects of the vacuum chamber walls on the plasma beam.

Plasma characteristics measurements have been performed with a Retarded Potential Analyzer (RPA).[39] The diagnostic setup has been set on a polar probing arm system. The system has been aligned on the axis of symmetry of the sources and with its origin at the exhaust plane. It allows the movement of the probe in a radial direction $r$ and a polar direction $\theta$, respectively in the 0 mm $< r <$ 400 mm range, and in the $-90° < \theta < 90°$ range. The step-motors have a resolution of 0.3 mm in the radial direction and 1° in the polar one. The RPA central axis has been aligned with the arm axis, and sweeps have been realised at a distance of 380 mm from the thruster exhaust plane, with angles in between $-50°$ and 50°. By measuring the electric current carried by positively charged ions, the RPA can provide the distribution function of ions' velocity and energy. The Semion Impedans RPA, hardware and software have been in use during the experiments. The derivative of the collected current is proportional to the Ion Energy Distribution Function (IEDF), thus the latter will be used to characterise the measurements of the RPA.

## 3. Results

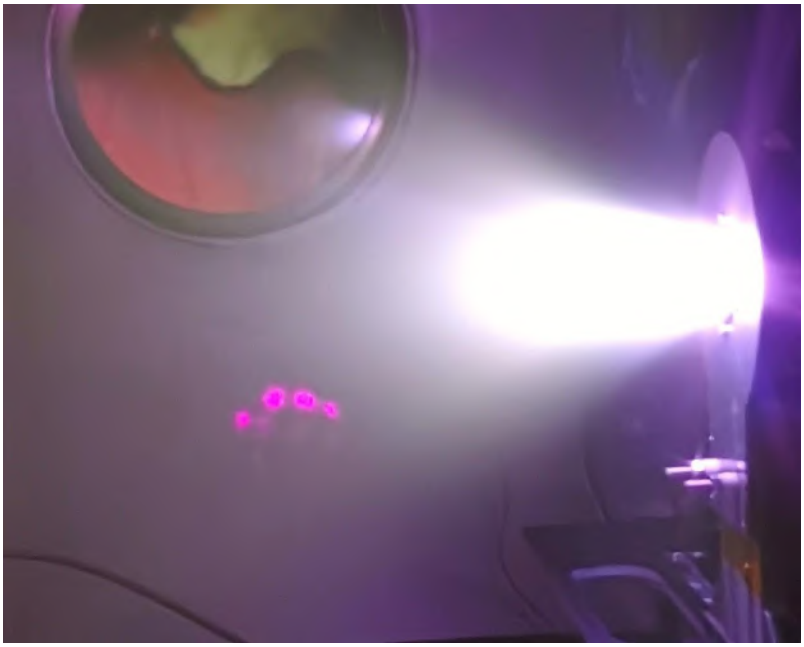

Figure 5: Single ECR source ignition with 25 sccm Krypton and 50 W. Nominal *MF ON* configuration ($I_{BC}$ = 11 A and $I_{MN}$ = 8.5 A) in use.

The optimisation of the source does not represent the main purpose of this work, thus the operation parameters were fixed throughout the measurements. Figure 5 depicts the plasma plume expansion out of a single source during ignition. Once the thruster is ignited with the *MF ON* configuration, it is possible to turn off the power supplies feeding the coils and to reach the *MF OFF* configuration. The latter represents the configuration in which plasma is produced without the presence of a magnetic field. The process which enables the transmission of microwave power in this configuration is therefore not the ECR.

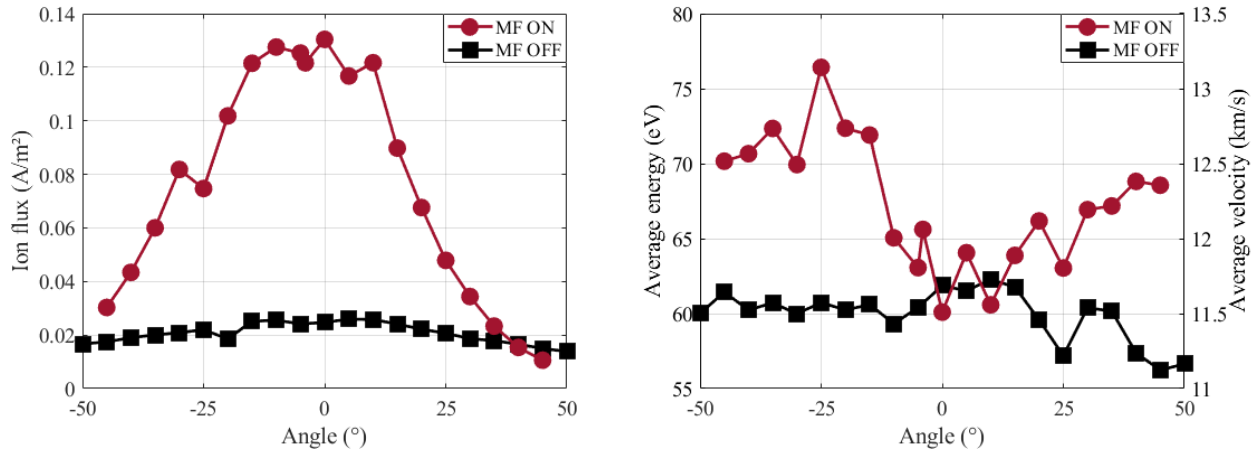


(a) Ion flux as a function of the azimuthal angle evolution for *MF ON* and *MF OFF*.

(b) Average ion energy and velocity as a function of the azimuthal angle for *MF ON* and *MF OFF*.

Figure 6: Ion flux, average ion energy and velocity as a function of the azimuthal angle, for both *MF ON* and *MF OFF* configurations. Conditions of operation: 7.5 sccm Krypton, 50 W, $I_{BC}$ = 11 A and $I_{MN}$ = 8.5 A.

RPA measurements have been operated with a single source thruster with the magnetic topologies *MF ON* and *MF OFF* defined in Section 2. IEDF measurements lead to Figure 6. Figure 6a illustrates the ion flux as a function of the angle for both *MF ON* and *MF OFF* configurations. *MF ON* configuration shows a single-peak ion flux. The ion flux peak occurs at 0.13 A/m$^2$ at the centre of the plasma beam. The *MF ON* ion flux curve displays minor asymmetries, which could be explained by the one-point gas injection - hence the asymmetric neutrals distribution in the IC. *MF OFF* ion flux is much lower, peaking around 0.02 A/m$^2$. As no magnetic field is applied to the thruster, ions are not guided any more by the magnetic nozzle. Logically, the collected current for this configuration decreases along the increase in angle, as the RPA drifts away from the plasma beam. Even though the two magnetic topologies differ by the presence of a magnetic expansion, their ion average energy and velocity are of the same order of magnitude. The decrease of ion average energy in the range $[-10°; 10°]$ could be explained by the physical presence of the coaxial cylinder, obstructing the plasma beam.

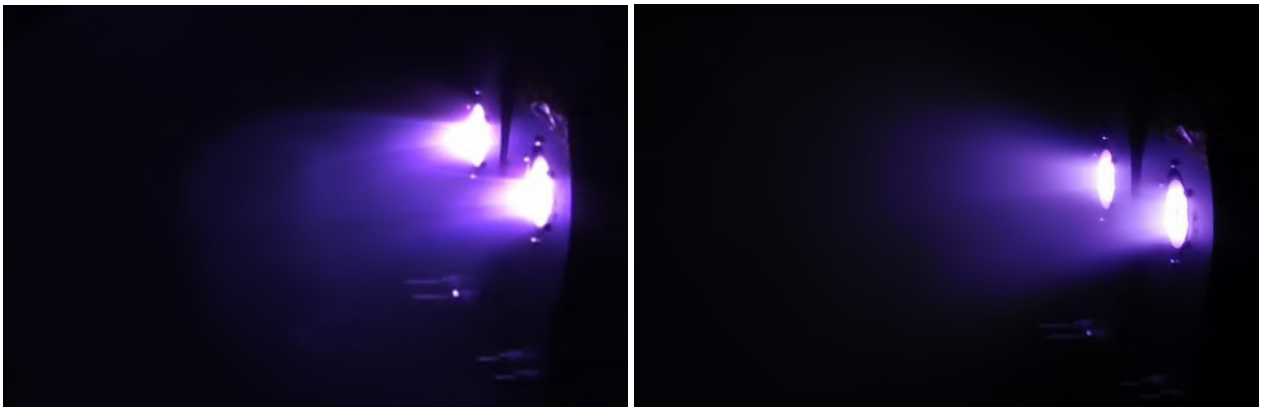

(a) Two ECR sources cluster in operation with 15 sccm Krypton and 100 W. *MF ARCH* magnetic topology ($I_{BC}$ = 11 A and $I_{MN}$ = 8.5 A) in use.

(b) Two ECR sources cluster in operation with 15 sccm Krypton and 100 W. *MF SAME* magnetic topology ($I_{BC}$ = 11 A and $I_{MN}$ = 8.5 A) in use.

Figure 7: Two ECR sources cluster in operation with *MF ARCH* and *MF SAME* magnetic configurations.

The two ECR sources cluster ignition and characterisation have taken place following the ones of the single source. Figure 7a displays the cluster in operation for the *MF ARCH* topology, with 15 sccm Krypton and an input MW power of 100 W shared between the two sources. A plasma arch linking the two sources can be observed, with a lower brightness than the plasma produced in the IC. Diverging plasma beams can be seen in Figure 7b for the *MF*

*SAME* configuration, as the magnetic field lines divaricate due to the polarisation of the electromagnetic coils. The brightness difference in the IC between Figure 7a and Figure 7b can be explained by the conditions in which the photos were taken. It is not representative of the plasma density of each of the magnetic topologies.

The Ion current density, ion average energy and velocity measured at the plume for the cluster configuration are displayed in Figure 8. Figure 8a proves ion current is extracted from the *MF ARCH* configuration, with a single peak. The amplitude of this peak is larger than the ones of the *MF SAME* and *MF OFF* configurations. Moreover, the divergence is the lowest for the *MF ARCH* configuration. A slight asymmetry is present for the ion flux of *MF ARCH* topology in Figure 8a, with a higher ion flux at $-5°$ (97 mA/m$^2$) than at $5°$ (93 mA/m$^2$). Regarding the *MF SAME* configuration, two peaks appear with 85 mA/m$^2$ at $-20°$ against 77 mA/m$^2$ at $20°$. These two peaks confirm the effect of the magnetic divergent field on the plasma expansion. An unequal gas distribution between the two sources can explain these asymmetries, as the gas line is divided by a Swagelock T-splitter before being brought to the IC. Moreover, different matching of the MW in each source could be an additional possible explanation. As for the single source in Figure 6a, the *MF OFF* topology remains around 20 mA/m$^2$ regardless of the measurement angle for both the single source and the cluster - even though the latter uses double the power and mass flow rate.

Figure 8b focuses on the ion average energy and velocity. The lowest average energy is found for *MF ARCH* topology. Ions escaping the closed-line magnetic field might be slowed down. *MF SAME* topology shows the same effects of the diverging field on both ion flux and average energy, with higher levels at $\pm 25°$. Finally, the *MF OFF* topology shows the highest ion average energy levels despite displaying the lowest ion flux. It is to be noted that the measured ion energy is directed in the perpendicular direction to the RPA. Thus, part of the ion kinetic energy could be not taken into account in the RPA scan.

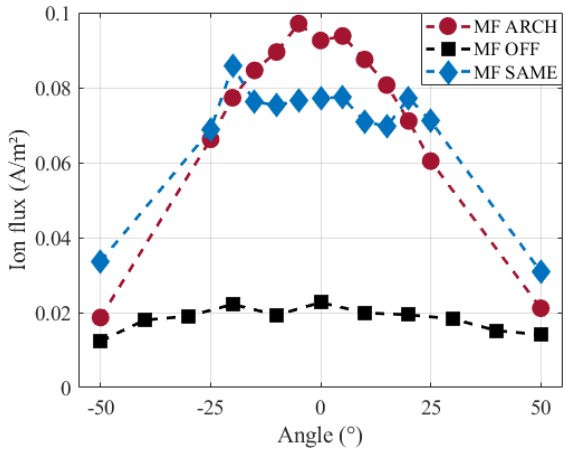


(a) Ion flux as a function of the azimuthal angle for *MF ARCH*, *MF SAME* and *MF OFF*.

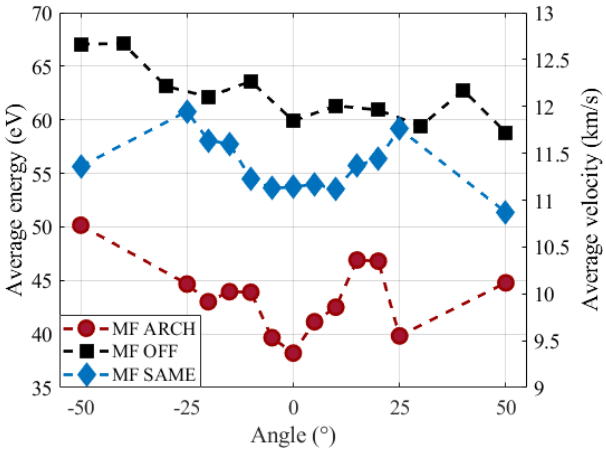


(b) Average ion energy and velocity as a function of the azimuthal angle for *MF ARCH*, *MF SAME* and *MF OFF*.

Figure 8: Ion flux, average ion energy and velocity as a function of the azimuthal angle, for both *MF ON* and *MF OFF* configurations. Conditions of operation: 15 sccm Krypton, 100 W, $I_{BC}$ = 11 A and $I_{MN}$ = 8.5 A.

## 4. Conclusion

The development and the preliminary characterisation of a two coaxial ECR sources cluster have been carried out. To begin with, a single source has been characterised with 7.5 sccm of Krypton and 50 W of MW power at 2.45 GHz. The total mass flow rate input in the cluster of two ECR sources has been increased up to 15 sccm, whilst the MW power has been set to 50 W. Several conclusions can be drawn from the measurements performed with the RPA.

The clustering of two ECR sources comes with two main magnetic topologies, characterised by the sources polarities. The closed-line topology formed when the sources have opposite polarity shows a decrease in divergence, with a single peak ion flux. This phenomenon has already been observed in simulation works.[37,40,41] The diverging magnetic topology achieved when sources are set with the same polarity deviates from the ion flux. This divergence could lower the performances of this topology, as the plasma beam is not centred on the thruster axis. Overall, RPA

measurements show the viability of a closed-line magnetic field topology in a cluster of two ECR coaxial sources. The investigation allows us to conclude that a plasma beam can indeed be extracted from a magnetic arch configuration: the presence of a magnetic field arch does not prevent plasma expansion or ions acceleration. It is to be noticed that the mass flow rate and the power in use in the cluster represent double the ones of the single source.

Moreover, the characterisation of a single source shows the necessity to use a multiple-point gas injection to reduce the plume asymmetry. A monotonically decreasing magnetic field would also be preferable to set a single resonance surface in the IC, possibly improving the performances of the source in terms of ionisation rate, power absorption and plasma expansion. The use of permanent magnets would help increase the operation time of the sources. Improvements and changes can be brought to the preliminary prototype of the two ECR sources cluster. In addition, exploring different inclinations of electromagnets and/or permanent magnets as well as modifying the distance between the sources could provide useful data on the interaction between the sources.

Further investigations are needed to achieve a better understanding of the plasma plume characteristics, with the use of Faraday cups (for ion current profile) or Langmuir probes (for plasma density, plasma potential or electron temperature). However, these intrusive measurement methods would only manage to indirectly define the ion acceleration. The use of non-intrusive measurement methods - such as LASER-Induced Fluorescence (LIF), and direct measurements - with a thrust balance, could help to more accurately assess the cluster performances and characteristics.

## Acknowledgments

This work has been carried out as part of the ZARATHUSTRA project, which has received funding from the European Research Council (ERC) under the European Union's Horizon 2020 research and innovation programme (Grant Agreement No.950466).

## References

[1] J. Boeuf, "Tutorial: Physics and modeling of Hall thrusters," *J. Applied Physics*, vol. 121, no. 1, p. 011101, 2017.

[2] E. Ahedo, "Plasmas for space propulsion," *Plasma Physics and Controlled Fusion*, vol. 53, no. 12, p. 124037, 2011.

[3] S. Mazouffre, "Electric propulsion for satellites and spacecraft: established technologies and novel approaches," *Plasma Sources Science and Technology*, vol. 25, no. 3, p. 033002, 2016.

[4] C. Charles and R. Boswell, "Current-free double-layer formation in a high-density helicon discharge," *Applied Physics Letters*, vol. 82, no. 9, pp. 1356–1358, 2003.

[5] O. Batishchev, "Minihelicon plasma thruster," *IEEE Transactions on Plasma Science*, vol. 37, no. 8, pp. 1563–1571, 2009.

[6] J. Navarro-Cavallé, E. Ahedo, M. Merino, V. Gómez, and M. Ruiz, "Helicon plasma thrusters: prototypes and advances on modeling," in $33^{rd}$ *International Electric Propulsion Conference*, no. IEPC-2013-285, Electric Rocket Propulsion Society, 2013.

[7] J. Navarro-Cavallé, "Helicon plasma thruster prototypes and modelling status," in *International Conference on Phenomena in Ionized Gases*, 2013.

[8] K. Takahashi, "Helicon–type radiofrequency plasma thrusters and magnetic plasma nozzles," *Reviews of Modern Plasma Physics*, vol. 3, p. 3, 2019.

[9] G. Bethke and D. Miller, "Cyclotron resonance thruster design techniques.," *AIAA Journal*, vol. 4, no. 5, pp. 835–840, 1966.

[10] R. Geller, *Electron cyclotron resonance ion sources and ECR plasmas*. CRC Press, 1996.

[11] T. Vialis, *Développement d'un propulseur plasma à résonance cyclotron électronique pour les satellites*. PhD thesis, SORBONNE UNIVERSITE, 2018.

[12] K. Takahashi, C. Charles, R. Boswell, and A. Ando, "Performance improvement of a permanent magnet helicon plasma thruster," *Journal of Physics D: Applied Physics*, vol. 46, no. 35, p. 352001, 2013.

[13] E. Ahedo and M. Merino, "On plasma detachment in propulsive magnetic nozzles," *Physics of Plasmas*, vol. 18, no. 5, p. 053504, 2011.

[14] M. Merino and E. Ahedo, "Magnetic nozzles for space plasma thrusters," in *Encyclopedia of Plasma Technology* (J. L. Shohet, ed.), vol. 2, pp. 1329–1351, Taylor and Francis, 2016.

[15] J. M. Little and E. Y. Choueiri, "Electron demagnetization in a magnetically expanding plasma," *Physical review letters*, vol. 123, no. 14, p. 145001, 2019.

[16] D. B. Miller, E. F. Gibbons, and D. J. B. Daniel, "Cyclotron resonance propulsion system," in *AIAA Electric Propulsion Conference*, p. 33, 1963.

[17] D. B. Miller and E. F. Gibbons, "Experiments with an electron cyclotron resonance plasma accelerator," *AIAA Journal*, vol. 2, pp. 35–41, Jan. 1964.

[18] G. Crimi, A. Eckert, and D. Miller, "Microwave driven magnetic plasma accelerator studies (cyclops)," tech. rep., General Electric Company, Space Sciences Laboratory, Missile and Space Division, 1967.

[19] M. Nagatomo, "Plasma acceleration by high frequency electromagnetic wave in staticmagnetic field gradient," in *6th Electric Propulsion and Plasmadynamics Conference*, p. 660, American Institute of Aeronautics and Astronautics, Sept. 1967.

[20] H. Kosmahl, "Three-dimensional plasma acceleration through axisymmetric diverging magnetic fields based on dipole moment approximation," tech. rep., NASA TN D-3782, 1967.

[21] J. Sercel, "Electron-cyclotron-resonance (ECR) plasma acceleration," in *AIAA 19th Fluid Dynamics, Plasma Dynamics and Lasers Conference*, 1987.

[22] J. Sercel, "Electron-cyclotron-resonance (ECR) plasma thruster research," in *24th Joint Propulsion Conference*, p. 2916, 1988.

[23] J. Sercel, "Simple model of plasma acceleration in a magnetic nozzle," in *21st International Electric Propulsion Conference*, vol. 1, 1990.

[24] J. Sercel, *An experimental and theoretical study of the ECR plasma engine*. PhD thesis, California Institute of Technology, 1993.

[25] J. Jarrige, P. Elias, F. Cannat, and D. Packan, "Performance comparison of an ECR plasma thruster using argon and xenon as propellant gas," in *33rd International Electric Propulsion Conference*, Paper 2013-420, (Washington D.C., October 7-10), Electric Rocket Propulsion Society, Fairview Park, OH, 2013.

[26] J. Jarrige, P. Elias, F. Cannat, and D. Packan, "Characterization of a coaxial ecr plasma thruster," in *44th AIAA Plasmadynamics and Lasers Conference, San Diego*, 2013.

[27] F. Cannat, J. Jarrige, P. Elias, and D. Packan, "Experimental investigation of magnetic gradient influence in a coaxial ECR plasma thruster," in *Space Propulsion Conference, Cologne, Germany*, 2014.

[28] F. Cannat, T. Lafleur, J. Jarrige, P. Chabert, P. Elias, and D. Packan, "Optimization of a coaxial electron cyclotron resonance plasma thruster with an analytical model," *Physics of Plasmas*, vol. 22, no. 5, p. 053503, 2015.

[29] V. Désangles and J. J. D. Packan, "Ecra thruster advances, 30w and 200w prototypes latest performances," in *IEPC 2022, Boston*, IEPC-2022-513, 2022.

[30] S. Peterschmitt and D. Packan, "Comparison of waveguide coupled and coaxial coupled ecra magnetic nozzle thruster using a thrust balance," in *Proc. of the 36th Int. Electric Propulsion Conf.(Vienna, Austria)*, pp. 2019–188, 2019.

[31] S. Peterschmitt and D. Packan, "Impact of the microwave coupling structure on an electron-cyclotron resonance thruster," *Journal of Propulsion and Power*, vol. 37, no. 6, pp. 806–815, 2021.

[32] M. R. Inchingolo, M. Merino, and J. Navarro-Cavallé, "Hybrid pic-fluid simulation of a waveguide ecr magnetic nozzle plasma thruster," in *Space Propulsion Conference 2021*, no. 00192, (March 17-19), Association Aéronautique et Astronautique de France, 2021.

[33] M. Inchingolo, J. Navarro-Cavallé, and M. Merino, "Design and plume characterization of a low-power circular waveguide coupled ecr thruster," in *5$^{th}$ International Workshop on Micropropulsion and CubeSats*, (Toulouse (online)), 2021.

[34] M. Merino, "Magnetic nozzles for electric propulsion," in *EPIC lecture series*, (Madrid, Spain), SRC EPIC, 2017.

[35] K. Vereen, A. Kimber, J. Correy, D. Olson, H. Martin, and R. Winglee, "Characterization of a cluster of high power helicon thrusters," in *AIAA Propulsion and Energy 2021 Forum*, AIAA 2017-4628, 2017.

[36] K. Vereen, J. Correy, H. Martin, K. Durkee, A. Kullman, S. Fraser, and R. Winglee, "Recent advances in the clustering of high power helicon thrusters," in *AIAA Propulsion and Energy 2019 Forum*, AIAA 2019-3902, 2019.

[37] S. Di Fede, M. Manente, P. Comunian, and M. Magarotto, "Magnetic nozzle performance in a cluster of helicon plasma thrusters," *(accepted for publication)*, no. June, pp. 1–21, 2023.

[38] M. R. Inchingolo, M. Merino, and J. Navarro-Cavallé, "Plume characterization of a waveguide ecr thruster," *Journal of Applied Physics*, vol. 133, no. 11, p. 113304, 2023.

[39] S. T. Lai and C. Miller, "Retarding potential analyzer: Principles, designs, and space applications," *AIP Advances*, vol. 10, no. 9, p. 095324, 2020.

[40] M. Merino, D. García-Lahuerta, C. Boyé, J. Navarro-Cavallé, and E. Ahedo, "Preliminary model of the plasma expansion in a magnetic arch thruster (and overview of the first prototype)," in 37$^{th}$ *International Electric Propulsion Conference*, no. IEPC-2022-423, (Boston, MA, June 19-23), Electric Rocket Propulsion Society, 2022.

[41] M. Merino, D. GarcÃa-Lahuerta, and E. Ahedo, "Plasma acceleration in a magnetic arch," *Plasma Sources Science and Technology*, vol. 32, p. 065005, jun 2023.